EURASIAN JOURNAL OF MATHEMATICAL AND COMPUTER APPLICATIONS
ISSN 2306–6172
Volume 12, Issue 4 (2024) 47 – 53

FRICTION FACTOR IN MICROCHANNELS WITH DIFFERENT BOUNDARY CONDITIONS

Gluzdov D.S., Gatapova E.Ya.

Abstract Most microfluidic devices are constructed with rectangular cross-section microchannels, where the aspect ratio significantly impacts the friction factor and, consequently, pressure losses. In this study, we investigate how the friction factor depends on the microchannel aspect ratio under different boundary conditions. The results demonstrate that, at the same Reynolds numbers, the lowest friction factor is consistently observed in square cross-section microchannels. However, the impact of the aspect ratio on the friction factor diminishes at high boundary slip lengths.

Key words: Slip length, numerical calculation, microfluidics, microstructures, hydrophobic surface, drag reduction.

AMS Mathematics Subject Classification: 76-06, 76M12, 76B75, 76Z99.

DOI: 10.32523/2306-6172-2024-12-4-47-53

1 Introduction

Microfluidic systems enable precise control over small fluid volumes, making them invaluable tools in biomedical and healthcare applications [1]. These systems are also used in areas such as disease detection and monitoring [2], environmental monitoring [3], food and agriculture [4], and the chemical and pharmaceutical industries [5]. The rapid advancement of microfluidic applications has created a need to improve microchannel properties and to identify the optimal materials, geometry, and boundary conditions for microchannels.

The objective of this study is to investigate the influence of aspect ratio on friction factors in microchannels under different boundary conditions. While many studies have examined the impact of varying microchannel cross-sections on friction factors [6], they typically consider only no-slip boundary conditions. In this study, we employed numerical calculations, which were validated for smooth microchannels using both analytical solutions presented here and comparisons with experimental data from our previous work [7]. Additionally, the calculations for microchannels with bubble mattress boundary conditions were compared with results from other authors.

2 Fluid flow in microchannels with different cross-sections and boundary conditions

Fig. 1 depicts two types of microchannels with different boundary conditions studied in this work. The most prevalent cross-section is usually circular, but rectangular and

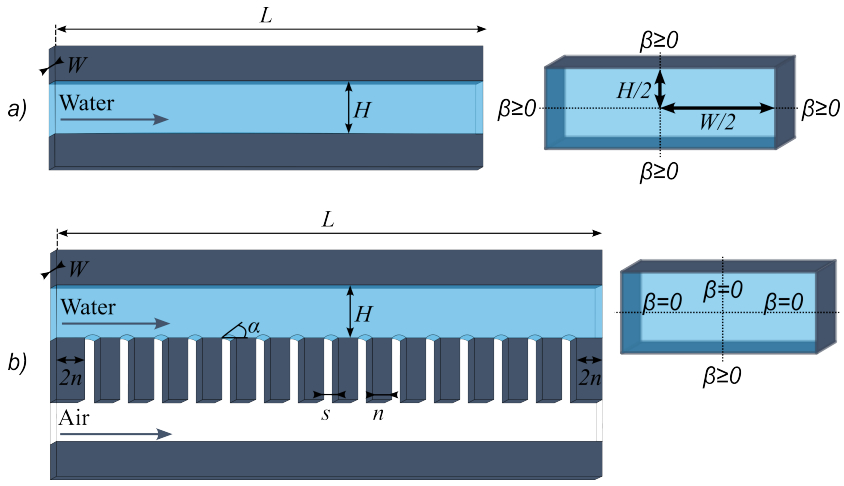

Figure 1: a) The rectangular cross-section smooth microchannel, b) the microchannel with controllable bubble mattress [8].

square cross-sections are most frequently utilized in microfluidic devices due to their superior suitability for microchips and enhanced material utilization.

One method for quantifying the flow throughput of a microchannel is the Darcy friction factor:

$$f = \Delta P \frac{2 D_h A^2}{\rho L Q^2}, \tag{1}$$

where D_h - the hydraulic diameter, L - the length of the channel, ΔP - the pressure drop, ρ - the density, Q - the flow rate and A - the cross-section area. The hydraulic diameter is $D_h = 4A/P$, where P - the wetted perimeter, for rectangular cross-section $D_h = 2WH/(W + H)$, where H - the microchannel height, W - the microchannel width.

The Reynolds number is calculated using the formula:

$$Re = D_h \frac{\rho}{\mu} \frac{Q}{A}, \tag{2}$$

where μ - is the dynamic viscosity.

$$\Delta P = \frac{4 \mu Q L}{W H^3 \left[1/3 - \frac{64H}{\pi^5 W} \tanh(\frac{\pi W}{2H})\right]}. \tag{3}$$

The friction factor coefficient is often presented in pairs with the Reynolds number. The friction factor on Reynolds number multiplication $Re \cdot f$ for a circular cross-section is equal to 64, for a square cross-section $Re \cdot f$ is approximately equal to 56, and for rectangular cross-sections, the value of $Re \cdot f$ can be calculated using the solution presented in [9]:

The formula (3) illustrates the dependence of pressure drop on fluid flow rate Q in rectangular cross-section microchannels for stationary incompressible laminar flow. This is not an exact solution, but the solution with only the first term of the Fourier expansion, which provides accurate enough results for practical applications. The exact solution was first published by Cornish [10].

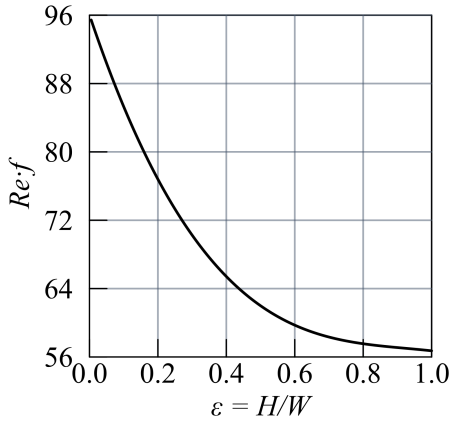

Figure 2: $Re \cdot f$ at different aspect ratios of rectangular cross-section channels.

Subsequently, the formulas (1)-(3) are combined into the value $Re \cdot f$ for rectangular cross-section microchannels:

$$Re \cdot f = \frac{96}{\left[1 - \frac{192H}{\pi^5 W} \tanh(\frac{\pi W}{2H})\right]} \frac{1}{(1 - \frac{H}{W})^2}. \tag{4}$$

Fig. 2 shows the dependence of $Re \cdot f$ on the aspect ratio H/W obtained by the formula (4). Formulas (3) and (4) are provided for the case of no-slip boundary conditions. In the case of microchannels, particularly those with superhydrophobic or structured surfaces, the Navier boundary condition is usually used:

$$u = \beta \left| \frac{\partial u}{\partial n} \right|, \tag{5}$$

where u - is the velocity near a boundary and n - is the normal to the boundary, β - the slip length. For $\beta > 0$ the formula (3) of the dependency of the pressure drop on fluid flow is given as:

$$\Delta P = \frac{12\mu QL}{1 + \frac{6\beta}{H} - \frac{192H}{\pi^5 W}(1 + \frac{\pi^2 \beta}{2H}) \tanh(\frac{\pi W}{2H})} \frac{1}{WH^3}. \tag{6}$$

This formula was obtained by substituting solution for velocity [10] into boundary condition as described in Watanabe work [11]. The coefficient of sliding friction β_{slid} used in the work [11] depends on slip length as $\beta_{slid} = \mu/\beta$ and in formula (6) slip length is used instead. Therefore $Re \cdot f$ can be found as:

$$Re \cdot f = \frac{96}{\left[1 + \frac{6\beta}{H} - \frac{192H}{\pi^5 W}(1 + \frac{\pi^2 \beta}{2H}) \tanh(\frac{\pi W}{2H})\right]} \frac{1}{(1 - \frac{H}{W})^2}. \tag{7}$$

In our previous work [12], we implemented Navier boundary conditions for numerical calculations, which were verified using formulas (6) and (7). The next section presents the results of the impact of slip length and bubble mattress boundary conditions on the friction factor.

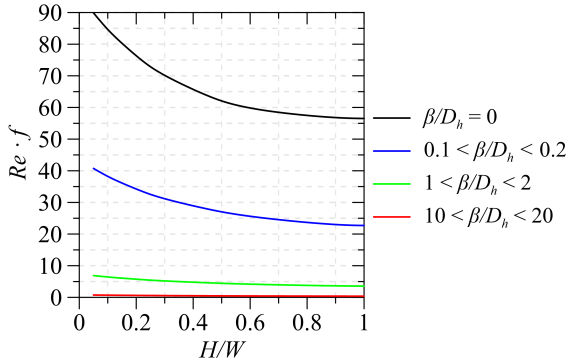

Figure 3: $Re \cdot f$ at different aspect ratios of rectangular cross-section microchannels depending on boundary slip length.

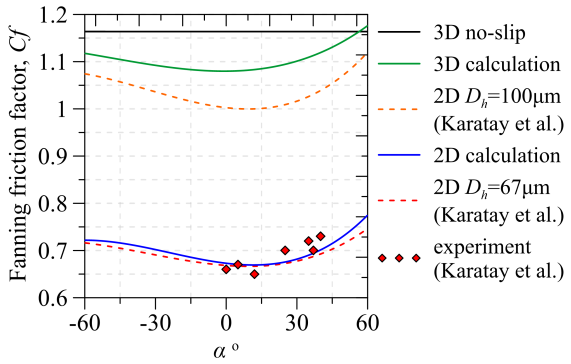

Figure 4: Fanning friction factor ($Cf = f/4$) obtained in 3D and 2D calculation compared with the work [8].

3 Results

In this work, the laminar 3D flow in a rectangular microchannel was simulated using the CFD SIMPLE method in Fluent. The microchannel grid was constructed using hexagonal elements, each with a side length of 1-2 μm. The inlet velocity profile was set to be flat, and the inlet calculation domain was extended to one microchannel length to allow the flow to fully develop, minimizing the influence of inlet conditions on fluid flow. The computational domain of the fluid in the microchannel with bubble mattress boundary condition included up to $5 \cdot 10^6$ elements. Mesh convergence was verified using the pressure drop parameter at the fixed bubble protrusion angle of $\alpha = 30^o$. The difference in pressure drop simulations with $1 \cdot 10^6$ and $4 \cdot 10^6$ elements was found to be slightly less than 1%. Fluid density and viscosity were set according to the values for water at room temperature.

The no-slip boundary condition was set on the walls, and no-shear condition was on the bubble mattress. For smooth microchannel, the Navier boundary condition (5) was set using UDF function [12].

Fig. 3 shows the results of numerical calculations for the smooth microchannel that were compared with analytical solutions based on the formula (7). Fig. 1 a) shows the scheme of the smooth microchannel. The results indicate that the smallest friction

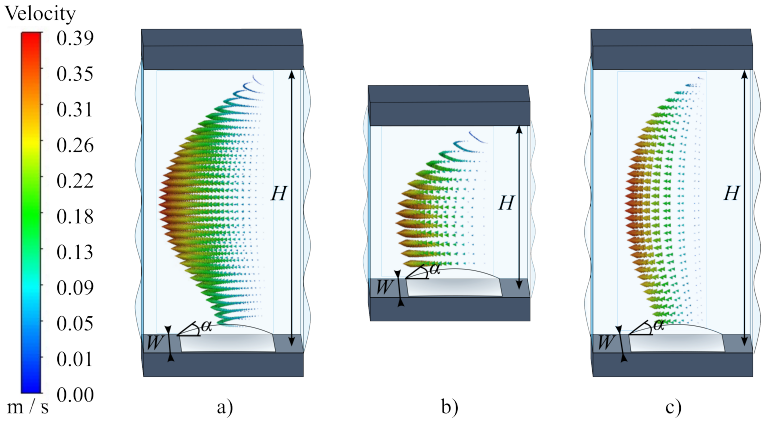

Figure 5: Velocity profiles in microchannels with $\alpha = 10^o$ at a) $H = 50\ \mu m$, $W = 100\ \mu m$, b) $H = 20\ \mu m$, $W = 100\ \mu m$, c) $H = 50\ \mu m$, $W = 25\ \mu m$.

factor is observed in square cross-section microchannels ($H/W = 1$). However, the influence of aspect ratio on friction factor decreases at higher slip lengths.

Next, we implemented a numerical calculation setup for complex boundary conditions with bubble mattresses (Fig. 1 b)). To identify robust and promising boundary structures for use in microchannels, a comprehensive literature review was conducted [13]. We found that certain setups could yield reliable results for investigations and potential applications in microfluidic devices. One such boundary structure is shown in Fig. 1 b) [8].

Fig. 4 presents the results of the Fanning friction factor ($Cf = f/4$) calculations in this study, compared with those from [8]. Karatay et al. used the PIV method to measure the friction factor at the center of the microchannel, achieving good agreement between experimental results and 2D simulation data. Our 2D simulation results also align well with their data. However, the 3D simulation results are not directly comparable to the 2D results. According to formulas (2) and (4) the friction factor in the 3D case with $H = 50\ \mu m$ and $W = 100\ \mu m$ is related to friction factor in the 2D case with $H = 50\ \mu m$ and $D_h = 100\ \mu m$ by a factor of 0,96. It should also be noted that in the 2D case, the slip area where bubbles are present is 23%, whereas in the 3D case, the slip area is only 14%, which is a 9% reduction. These results indicate that 3D calculations differ from 2D calculations primarily due to the influence of side walls on fluid flow in the 3D case, particularly when the slip condition on the bubbles is considered.

Fig. 5 - Fig. 7 illustrate the results of the fluid flow 3D calculation within the microchannel with bubble mattress boundary condition (Fig. 1 b)). The results shown in Fig. 5 were obtained in the middle of the main domain of the microchannel near the bubbles. Fig. 5 is given to illustrate how the flow profile changes in a microchannel with a bubble layer at different aspect ratios of the microchannel during three-dimensional calculations. For Fig. 5 - Fig. 7 the bubble width $s = 30\ \mu m$, the distance between bubbles $n = 20\ \mu m$ (Fig. 1 b)), the average water velocity $U_{in} = 0.2\ m/s$ at the inlet of the microchannel. The width and height of the microchannel were varied.

Fig. 6 and Fig. 7 demonstrate that the minimal friction factor is observed at the

square cross-section when $H = W = 50\ \mu m$ (Fig. 6) or $H = W = 100\ \mu m$ (Fig. 7). The bubble protrusion angle (Fig. 4, Fig. 1 b)) negatively affects the friction factor, and the optimal protrusion angle is observed to be near $\alpha = 0^o$.

4 Conclusion

In this study, we examined the influence of microchannel dimensions, aspect ratio, slip length, and boundary structures on the Darcy friction factor.

We presented analytical equations that can be used to compare numerical calculations for simplified microchannel configurations with analytical solutions for incompressible laminar stationary fluid flow in rectangular cross-section microchannels with Navier boundary conditions. These analytical solutions are not commonly found in the literature and may be valuable for applications beyond the scope of this work.

Our numerical investigations indicate that the friction factor primarily depends on the cross-sectional aspect ratio of the microchannels. However, the influence of the aspect ratio on the friction factor diminishes when a slip boundary condition is applied.

For microchannels with bubble mattress boundary conditions, the aspect ratio has a stronger impact on the friction factor, especially at high bubble protrusion angles. As the bubble protrusion angle increases, the friction factor can rise significantly, resulting in reduced microchannel throughput. To mitigate the influence of bubble height instability on the friction factor, it is recommended to use microchannels with higher aspect ratios.

Acknowledgement

This study was supported by the Russian Science Foundation Project No. 20-19-00722, https://rscf.ru/en/project/20-19-00722/.

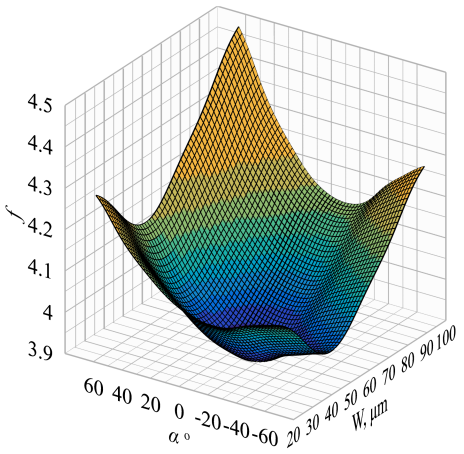

Figure 6: Friction factor at different bubble protrusion angles and microchannel widths. $H = 50\ \mu m$.

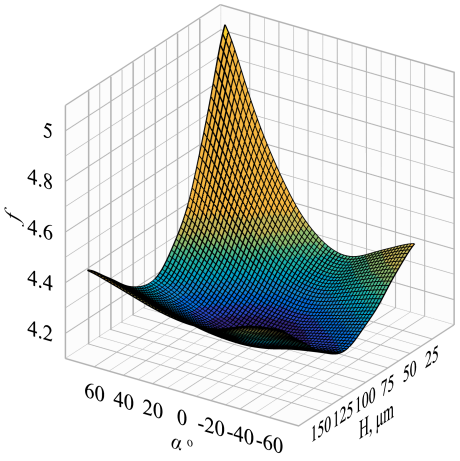

Figure 7: Friction factor at different bubble protrusion angles and microchannel heights. $W = 100\ \mu m$.

References

[1] Dong R. et al., *Microfluidics-Based Biomaterials and Biodevices*, Advanced Materials. Wiley-VCH Verlag, Vol. 31, Issue 45, 2019.

[2] Kaushik A.M., Hsieh K., Wang T.H., *Droplet microfluidics for high-sensitivity and high-throughput detection and screening of disease biomarkers*, Wiley Interdisciplinary Reviews: Nanomedicine and Nanobiotechnology. Wiley-Blackwell, Vol. 10, Issue 6, 2018.

[3] Jaywant S.A., Mahmood Arif K., *A comprehensive review of micro fluidic water quality monitoring sensors*, Sensors (Switzerland). MDPI AG, Vol. 19, Issue 21, 2019.

[4] Weng X., Neethirajan S., *Ensuring food safety: Quality monitoring using microfluidics*, Trends in Food Science and Technology. Elsevier Ltd, Vol. 65, 2017, pp. 10-22.

[5] Liu Y. et al. , *Microfluidics for Drug Development: From Synthesis to Evaluation*, Chemical Reviews. American Chemical Society, Vol. 121, Issue 13, 2021, pp. 7468-7529.

[6] Bahrami M., Yovanovich M.M., Culham J.R., *Pressure drop of fully-developed, laminar flow in microchannels of arbitrary cross-section*, International Conference on Nanochannels, Microchannels, and Minichannels, Vol. 41855, 2005.

[7] Gluzdov, D.S. and Gatapova, E.Ya., *Friction reduction by inlet temperature variation in microchannel flow*, Physics of Fluids, Vol. 33, Issue 6, 2021.

[8] Karatay E., Haase A., Visser C., et al., *Control of slippage with tunable bubble mattresses*, Proceedings of the National Academy of Sciences, Vol. 110, Issue 21, 2013, pp. 8422-8426.

[9] White F.M. and Majdalani J., *Viscous fluid flow*, McGraw-Hill New York, Vol. 3, 2006, ch. 3, p. 120.

[10] Cornish R.J., *Flow in a pipe of rectangular cross-section*, Proceedings of the Royal Society of London. Series A, Containing Papers of a Mathematical and Physical Character, Vol. 120, 1928, n. 786, pp. 525-529.

[11] Watanabe K., Mizunuma H., et al., *Slip of netwonian fluids at slid boundary*, JSME International Journal Series B Fluids and Thermal Engineering. MDPI AG, Vol. 41, 1998, pp. 525-529.

[12] Gluzdov D.S., Gatapova E.Ya., *Numerical implementation of boundary conditions on bubbles in a microchannel with stationary laminar flow*, Journal of Engineering Thermophysics, 2024.

[13] Gluzdov D.S. and Gatapova E.Ya., *Microchannel surface structures for drag reduction*, Journal of Engineering Thermophysics, Vol. 32, Issue 2, 2023, pp. 214-241.

D.S. Gluzdov,
Kutateladze Institute of Thermophysics SB RAS,
1, Lavrentyev avenue, 630090, Novosibirsk, Russia;
Novosibirsk State University,
1, Pirogova str., 630090, Novosibirsk, Russia,
Email: `d.gluzdov@g.nsu.ru`

E.Ya. Gatapova,
Kutateladze Institute of Thermophysics SB RAS,
1, Lavrentyev avenue, 630090, Novosibirsk, Russia;
Novosibirsk State University,
1, Pirogova str., 630090, Novosibirsk, Russia,
Email: `gatapova@itp.nsc.ru`

Received 11.08.2024, Accepted 02.10.2024